Eur. Phys. J. E (2012) **35**: 5
DOI 10.1140/epje/i2012-12005-2

THE EUROPEAN PHYSICAL JOURNAL E

Regular Article

Elastic contact mechanics: Percolation of the contact area and fluid squeeze-out

B.N.J. Persson[1,a], N. Prodanov[1,2], B.A. Krick[3], N. Rodriguez[4], N. Mulakaluri[1], W.G. Sawyer[3], and P. Mangiagalli[5]

[1] IFF, FZ Jülich, D-52425 Jülich, Germany
[2] Sumy State University, 2 Rimskii-Korsakov Str., 40007 Sumy, Ukraine
[3] Department of Mechanical and Aerospace Engineering, University of Florida, Gainesville FL 32611, USA
[4] Advanced Technologies, BD Medical-Pharmaceutical Systems, 1 Becton Drive, MC 427, Franklin Lakes, NJ 07417, USA
[5] Advanced Technologies, BD-Pharmaceutical Systems, 38800 Pont de Claix, France

Received 7 November 2011 and Received in final form 5 January 2012
Published online: 26 January 2012 –

Abstract. The dynamics of fluid flow at the interface between elastic solids with rough surfaces depends sensitively on the area of real contact, in particular close to the percolation threshold, where an irregular network of narrow flow channels prevails. In this paper, numerical simulation and experimental results for the contact between elastic solids with isotropic and anisotropic surface roughness are compared with the predictions of a theory based on the Persson contact mechanics theory and the Bruggeman effective medium theory. The theory predictions are in good agreement with the experimental and numerical simulation results and the (small) deviation can be understood as a finite-size effect. The fluid squeeze-out at the interface between elastic solids with randomly rough surfaces is studied. We present results for such high contact pressures that the area of real contact percolates, giving rise to sealed-off domains with pressurized fluid at the interface. The theoretical predictions are compared to experimental data for a simple model system (a rubber block squeezed against a flat glass plate), and for prefilled syringes, where the rubber plunger stopper is lubricated by a high-viscosity silicon oil to ensure functionality of the delivery device. For the latter system we compare the breakloose (or static) friction, as a function of the time of stationary contact, to the theory prediction.

1 Introduction

The influence of surface roughness on fluid flow at the interface between solids in stationary or sliding contact is a topic of great importance both in nature and technology. Technological applications include leakage of seals, mixed lubrication, and removal of water from the tire-road footprint. In nature, fluid removal (squeeze-out) is important for adhesion and grip between the tree frog or gecko adhesive toe pads and the countersurface during raining, and for cell adhesion.

Almost all surfaces in nature and most surfaces of interest in tribology have roughness on many different length scales, sometimes extending from atomic distances ($\sim$ 1 nm) to the macroscopic size of the system which could be of order $\sim$ 1 cm. Often the roughness is fractal-like so that when a small region is magnified (in general with different magnification in the parallel and orthogonal directions) it "looks the same" as the unmagnified surface.

Most objects produced in engineering have some particular macroscopic shape characterized by a radius of curvature (which may vary over the surface of the solid) *e.g.*, the radius R of a cylinder in a combustion engine. In this case the surface may appear perfectly smooth to the naked eye, but at short enough length scale, in general much smaller than R, the surface will exhibit strong irregularities (surface roughness). The surface roughness power spectrum $C(\mathbf{q})$ of such a surface will exhibit a roll-off wavelength $\lambda_0 \ll R$ (related to the roll-off wave vector $q_0 = 2\pi/\lambda_0$) and will appear smooth (except for the macroscopic curvature R) on length scales much longer than λ_0. In this case, when studying the fluid flow between two macroscopic solids, one may homogenize the microscopic fluid dynamics occurring at the interface, resulting in effective fluid flow equations describing the average fluid flow on length scales much larger than λ_0, and which can be used to study, *e.g.*, the lubrication of the cylinder in an engine. This approach of eliminating or integrating out short length scale degrees of freedom to obtain effective equations of motion which describe the long distance (or slow) behavior is a very general and powerful concept often used in physics, and is employed in the study presented below.

[a] e-mail: b.persson@fz-juelich.de

In the context of fluid flow at the interface between closely spaced solids with surface roughness, Patir and Cheng [1,2] have shown how the Navier-Stokes equations of fluid dynamics can be reduced to effective equations of motion involving locally averaged fluid pressure and flow velocities. In the effective equation the so-called flow factors occur, which are functions of the locally averaged interfacial separation $\bar{u}$. The authors showed how the flow factors can be determined by solving numerically the fluid flow in small rectangular units with linear size of order of (or larger than) the roll-off wavelength λ_0 introduced above, and by averaging over several realizations. However, with the present speed (and memory) limitations of computers fully converged solutions using this approach can only take into account roughness over two or at most three decades in length scale. In addition, Patir and Cheng did not include the long-range elastic deformations of the solid walls in the analysis. Later studies have attempted to include elastic deformation using asperity contact mechanics models as pioneered by Greenwood-Williamson (GW) [3], but it is now known that this theory (and other asperity contact models [4]) does not accurately describe contact mechanics because of the neglect of the long-range elastic coupling between the asperity contact regions [5,6]. In particular, the relation between the average interfacial separation $\bar{u}$ and the squeezing pressure p, which is very important for the fluid flow problem, is not accurately described by the GW model [7–9].

The paper by Patir and Cheng was followed by many other studies of how to eliminate or integrate out the surface roughness in fluid flow problems (see, *e.g.*, the work by Sahlin *et al.* [10]). Most of these theories involve solving numerically the fluid flow in rectangular interfacial units and, just as in the Patir and Cheng approach, cannot include roughness on more than ~ 2 decades in length scale. In addition, in some of the studies the measured roughness topography must be "processed" in a non-trivial way in order to obey periodic boundary conditions (which is necessary for the Fast Fourier Transform method used in some of these studies).

Tripp [11] has presented an analytical derivation of the flow factors for the case where the separation between the surfaces is so large that no direct solid-solid contact occurs. He obtained the flow factors to first order in $\langle h^2\rangle/\bar{u}^2$, where $\langle h^2\rangle$ is the ensemble average of the square of the roughness amplitude and $\bar{u}$ is the average surface separation. The result of Tripp has recently been generalized to include elastic deformations of the solids [12,13].

In this paper, the study of fluid squeeze-out from the region between two elastic solids with randomly rough surfaces is presented. We focus on such high contact pressures that after long enough contact time the area of real contact percolates resulting in pockets of confined, pressurized, fluid at the interface. The Bruggeman effective medium theory and the Persson contact mechanics theory are employed to calculate the interfacial fluid conductivity tensor. For anisotropic surface roughness the Bruggeman effective medium theory predicts that the contact area percolates when $A/A_0 = \gamma/(1+\gamma)$, where γ is the Peklenik number (the ratio between the decay length of the height-height correlation function along the two principle directions) and A/A_0 is the relative contact area (A_0 is the nominal or apparent contact area). The main aim of the present work is to verify the theory predictions through the comparison with the results of molecular dynamics (MD) simulations and experiments. MD calculations have been carried out both for isotropic and anisotropic surface roughness, while the experiments consider only the surfaces with isotropic statistical properties (where $\gamma = 1$). The paper outline is as follows. The theoretical approach and its application to the fluid squeeze-out are described in sects. 2–4 and 5, respectively. Sections 6 and 7 present simulations and experiments. In sect. 8 we apply the theory to the breakloose (or static) friction for prefillable syringes. The work is closed by the concluding sect. 9.

2 Anisotropic surface roughness

Many surfaces of practical importance have roughness with isotropic statistical properties, *e.g.*, sandblasted surfaces or surfaces coated with particles typically bound by a resin to an otherwise flat surface, *e.g.*, sandpaper surfaces. However, some surfaces of engineering interest have surface roughness with anisotropic statistical properties, *e.g.*, surfaces which have been polished or grinded in one direction. The surface anisotropy is usually characterized by a single number, the so-called Peklenik number γ, which is the ratio between the decay length ξ_x and ξ_y of the height-height correlation function $\langle h(x,y)h(0,0)\rangle$ along the x- and y-directions, respectively, *i.e.* $\gamma = \xi_x/\xi_y$. Here it has been assumed that the x-axis is oriented along one of the principal directions of the anisotropic surface roughness.

Let us define the 2×2 matrix (we use polar coordinates so that the wave vector $\mathbf{q} = q(\cos\phi, \sin\phi)$) [13]

$$D(q) = \frac{\int \mathrm{d}\phi\ C(\mathbf{q})\mathbf{q}\mathbf{q}/q^2}{\int \mathrm{d}\phi\ C(\mathbf{q})}, \tag{1}$$

where the surface roughness power spectrum [14]

$$C(\mathbf{q}) = \frac{1}{(2\pi)^2}\int \mathrm{d}^2x\ \langle h(\mathbf{x})h(\mathbf{0})\rangle \mathrm{e}^{-i\mathbf{q}\cdot\mathbf{x}}, \tag{2}$$

where $\langle ...\rangle$ stands for ensemble average, and $h(\mathbf{x})$ is the height profile. For roughness with isotropic statistical properties, $C(\mathbf{q})$ will only depend on $q = |\mathbf{q}|$ and in this case $D(q)$ will be diagonal with $D_{11} = D_{22} = 1/2$.

We will assume most of the time that $D(q)$ is independent of q and in this case (1) is equivalent to

$$D = \frac{\int \mathrm{d}^2q\ C(\mathbf{q})\mathbf{q}\mathbf{q}/q^2}{\int \mathrm{d}^2q\ C(\mathbf{q})}. \tag{3}$$

In this case, in the coordinate system where D is diagonal the flow conductivity matrix (defined below) σ_{eff} will be diagonal too. Note that $\mathrm{Tr}D = D_{11} + D_{22} = 1$, and in the coordinate system where D is diagonal we can write $D_{11} = 1/(1+\gamma)$ and $D_{22} = \gamma/(1+\gamma)$, where $\gamma = \xi_x/\xi_y$

is the Peklenik number. Note that $D_{11}(1/\gamma) = D_{22}(\gamma)$. If $D(q)$ (see (1)) depends on q we may still define (in the coordinate system where $D(q)$ is diagonal) $\gamma = -1+1/D_{11}$ as before, but the xy-coordinate system where $D(q)$ is diagonal may depend on q (in which case the rotation angle, $\psi(q)$, of the x-axis relative to some fixed axis, is important information too, see ref. [13]). In this case γ will depend on q and we will refer to $\gamma(q)$ as the Peklenik function (and $\psi(q)$ as the Peklenik angle function). Note that since $D(q)$ is a symmetric tensor and since $\mathrm{Tr}D = 1$, the D-matrix has only two independent components. Thus, it is fully defined by the Peklenik function $\gamma(q)$ and the Peklenik angle function $\psi(q)$. In this paper we will assume that $\gamma(q)$ and $\psi(q)$ are constant.

3 Fluid flow between solids with random surface roughness

Consider two elastic solids with randomly rough surfaces. Even if the solids are squeezed in contact, because of the surface roughness there will in general be non-contact regions at the interface and, if the squeezing force is not too large, there will exist non-contact channels from one side to the other side of the nominal contact region. We consider now fluid flow at the interface between the solids. We assume that the fluid is Newtonian and that the fluid velocity field $\mathbf{v}(\mathbf{x}, t)$ satisfies the Navier-Stokes equation

$$\frac{\partial \mathbf{v}}{\partial t} + \mathbf{v} \cdot \nabla \mathbf{v} = -\frac{1}{\rho}\nabla p + \nu \nabla^2 \mathbf{v},$$

where $\nu = \eta/\rho$ is the kinetic viscosity and ρ is the mass density. For simplicity we will also assume an incompressible fluid so that

$$\nabla \cdot \mathbf{v} = 0.$$

We assume that the non-linear term $\mathbf{v} \cdot \nabla \mathbf{v}$ can be neglected (this corresponds to small inertia and small Reynolds number), which is usually the case in fluid flow between narrowly spaced solid walls. For simplicity we assume the lower solid to be rigid with a flat surface, while the upper solid is elastic with a rough surface, see fig. 1. We introduce a coordinate system xyz with the xy-plane in the surface of the lower solid and the z-axis pointing towards the upper solid. Consider now squeezing the solids together in a fluid. Let $u(x, y, t)$ be the separation between the solid walls and assume that the slope $|\nabla u| \ll 1$. We also assume that $u/L \ll 1$, where L is the linear size of the nominal contact region. In this case one expects that the fluid velocity varies slowly with the coordinates x and y as compared to the variation in the orthogonal direction z. Assuming also a slow time dependence, the Navier-Stokes equation is reduced to

$$\eta \frac{\partial^2 \mathbf{v}}{\partial z^2} = \nabla p. \tag{4}$$

Here and in what follows $\mathbf{v} = (v_x, v_y)$, $\mathbf{x} = (x, y)$ and $\nabla = (\partial_x, \partial_y)$ are two-dimensional vectors. Note that $v_z \approx 0$ and

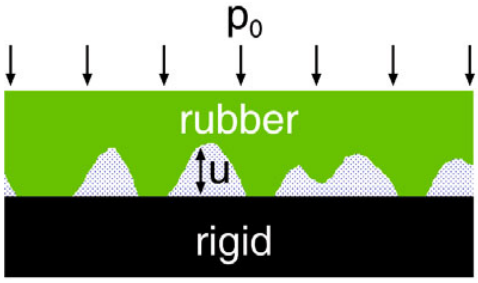

Fig. 1. An elastic solid (block) with a rough surface is squeezed (pressure p_0) in a fluid against a rigid solid (substrate) with a flat surface.

that $p(\mathbf{x})$ is independent of z to a good approximation. From (4) one can obtain the fluid flow vector

$$\mathbf{J} = -\frac{u^3(\mathbf{x})}{12\eta}\nabla p. \tag{5}$$

Assuming an incompressible fluid mass conservation demands that

$$\frac{\partial u(\mathbf{x}, t)}{\partial t} + \nabla \cdot \mathbf{J} = 0, \tag{6}$$

where the interfacial separation $u(\mathbf{x}, t)$ is the volume of fluid per unit area. In this last equation we have allowed for a slow time dependence of $u(\mathbf{x}, t)$ as would be the case, *e.g.*, during fluid squeeze-out from the interfacial region between two solids.

The fluid flow at the interface between contacting solids with surface roughness on many length scales is a very complex problem, in particular at high squeezing pressures where a network of flow channels with rapidly varying width and height may prevail at the interface. This is illustrated in fig. 2, which shows the contact area (black) between two elastic solids with randomly rough surfaces. At high enough pressure the contact area will percolate, which will have a drastic influence on the interfacial fluid flow properties. Percolation corresponds to the moment when the narrowest channel disappears as a result of squeezing. It is also visible that for anisotropic roughness percolation occurs later in the direction of the roughness elongation (which is vertical in fig. 2).

Equations (5) and (6) describe the fluid flow at the interface between contacting solids with rough surfaces. One can show that after eliminating all the surface roughness components, the fluid current (given by (5)) takes the form

$$\bar{\mathbf{J}} = -\sigma_{\mathrm{eff}} \nabla \bar{p}, \tag{7}$$

where $\bar{p}$ is the fluid pressure averaged over different realizations of the rough surface. The flow conductivity $\sigma_{\mathrm{eff}}(\bar{u})$ is in general (for anisotropic surface roughness) a 2×2 matrix. The ensemble average of (6) gives

$$\frac{\partial \bar{u}(\mathbf{x}, t)}{\partial t} + \nabla \cdot \bar{\mathbf{J}} = 0. \tag{8}$$

Substituting (7) in (8) gives

$$\frac{\partial \bar{u}(\mathbf{x}, t)}{\partial t} = \nabla \cdot (\sigma_{\mathrm{eff}} \nabla \bar{p}) \,. \tag{9}$$

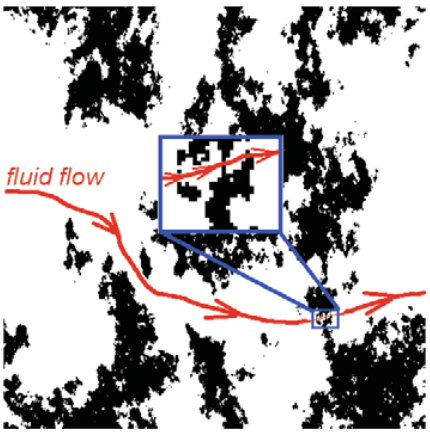

Fig. 2. (Color online) A snapshot of the contact before percolation in the x-direction (which is horizontal) for anisotropic roughness with Peklenik number 5/7. Red line indicates a fluid flow stream line. It is visible that fluid is able to flow from the left to the right part of the figure (or vice-versa) due to the presence of a narrow channel at some region of the contact. Inset presents the magnification of this region.

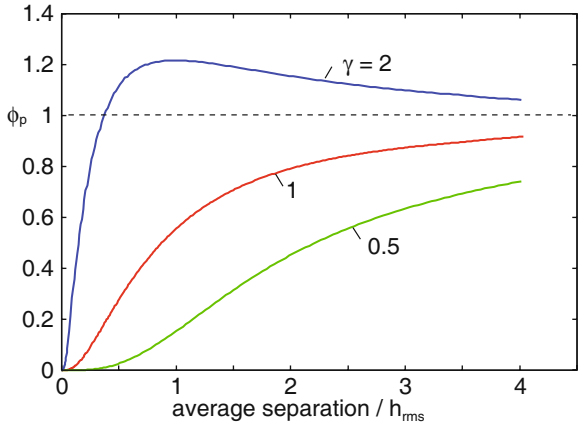

Fig. 3. (Color online) The pressure flow factor ϕ_p as a function of the average interfacial separation $\bar{u}$, for anisotropic surfaces with the Peklenik numbers $\gamma = 1/2$, 1 and 2. In all cases the angular average power spectrum is of the type shown in fig. 4 with $H = 0.9$ and the root-mean-square roughness $h_{rms} = 10\ \mu$m.

4 Fluid flow conductivity σ_{eff}

As was mentioned above, the fluid flow at the interface between contacting randomly rough surfaces requires taking into account the presence of the network of many interconnected flow channels. In a macroscopic approach this can be achieved through the use of the pressure flow factor. Here we have employed the 2D Bruggeman effective medium theory [15–18] to calculate (approximately) the pressure flow factor (see also appendix B).

For an anisotropic system, the effective medium flow conductivity σ_{eff} is a 2×2 matrix. Let us introduce a xy coordinate system and choose the x-axis along a principal axis of the D-matrix. In this case we can consider σ_{eff} as a scalar which within the Bruggeman effective medium theory satisfies the relation:

$$\frac{1}{\sigma_{eff}} = \int du\ P(u) \frac{1+\gamma}{\gamma\sigma_{eff} + \sigma(u)}, \tag{10}$$

where $P(u)$ is the probability distribution of interfacial separations, and where

$$\sigma(u) = \frac{u^3}{12\eta_0}. \tag{11}$$

Fluid flow along the y-axis is given by a similar equation with γ replaced with $1/\gamma$. The probability distribution $P(u)$ of interfacial separations has been derived in ref. [21]. Here we note that $P(u)$ has a delta function at the origin $u = 0$ with the weight determined by the area of real contact:

$$P(u) = \frac{A}{A_0}\delta(u) + P_c(u), \tag{12}$$

where $P_c(u)$ is a continuous (finite) function of u. Substituting this in (10) gives

$$\frac{1}{\sigma_{eff}} = \frac{A}{A_0}\frac{1+\gamma}{\gamma\sigma_{eff}} + \int du\ P_c(u) \frac{1+\gamma}{\gamma\sigma_{eff} + \sigma(u)}. \tag{13}$$

This equation is easy to solve by iteration.

In fig. 3 the pressure flow factor $\phi_p = 12\eta_0\sigma_{eff}/\bar{u}^3$ as a function of the average interfacial separation $\bar{u}$ is displayed for anisotropic surfaces with the Peklenik numbers $\gamma = 1/2$, 1 and 2 (see also below). Note that $\phi_p = 0$ for $\bar{u} < \bar{u}_c$, where $\bar{u}_c$ is the average interfacial separation where the area of real contact percolates in the direction orthogonal to the fluid flow. In the Bruggeman effective medium theory this occurs when the area of real contact equals $A/A_0 = \gamma/(\gamma+1)$. Thus for $\gamma = 1/2$, 1 and 2 the contact area percolates (so that no fluid flow occurs along the considered direction) when $A/A_0 = 1/3$, $1/2$ and $2/3$, respectively. This explains why ϕ_p vanishes at much larger (average) interfacial separation (and hence smaller contact area) for $\gamma = 1/2$ as compared to $\gamma = 2$.

In obtaining the results presented below we have used the Persson contact mechanics theory for the contact area A and the probability distribution $P(u)$ (see refs. [19–21]). This theory depends on the elastic energy U_{el} stored in the asperity contact regions and in this paper we use the simplest version for U_{el} (see ref. [5]), where the γ-parameter (not the Peklenik number) $= 1$. Comparison of the theory predictions with numerical simulations for small systems have shown that $\gamma \approx 0.45$ gives the best agreement between theory and the (numerical) experiments. However, using $\gamma = 0.45$ (or $\gamma \neq 1$ in general) results in much longer computational time, with relatively small numerical changes as compared to using $\gamma = 1$.

For large (average) surface separation $\bar{u}$ eqs. (5) and (6) can be solved exactly to leading order in $\langle h^2\rangle/\bar{u}^2$ (where $\langle h^2\rangle$ is the mean of the square of the surface rough-

ness amplitude $h(x,y)$, where we have assumed $\langle h\rangle = 0$) [11,13]

$$\phi_{\rm p} = 1 + \frac{3\langle h^2\rangle}{\bar{u}^2}(1-3D).$$

In appendix A we show that the Bruggeman effective medium theory gives the same expression for $\phi_{\rm p}$ to leading order in $\langle h^2\rangle/\bar{u}^2$ if we identify the γ-parameter in the effective medium theory with the Peklenik γ defined by the D-matrix (see sect. 2). This result shows that the parameter γ in the effective medium theory, which was introduced in a phenomenological way (as the ratio between the principle axis of an elliptic inclusion) in the effective medium theory (see ref. [13]), is indeed determined by the eigenvalues of the D-matrix as discussed in sect. 2. This is a very important result and completes the theory for $\sigma_{\rm eff}$ developed in ref. [13].

5 Fluid squeeze-out

Let us squeeze a rectangular rubber block (height d, width (x-direction) $2a$ and infinite length (y-direction)) against a substrate in a fluid. Assume that we can neglect the macroscopic deformations of the rubber block in response to the (macroscopically) non-uniform fluid pressure (which requires $d \ll a$) [22,23]. In this case $\bar{u}(\mathbf{x},t)$ will only depend on time t. For this case from (9) we get

$$\frac{{\rm d}\bar{u}}{{\rm d}t} - \frac{\bar{u}^3\phi_{\rm p}(\bar{u})}{12\eta}\frac{\partial^2\bar{p}}{\partial x^2} = 0.$$

It follows from this equation above that the fluid pressure is parabolic

$$\bar{p}(x,t) = \frac{3}{2}p_{\rm fluid}(t)\left(1-\frac{x^2}{a^2}\right),$$

where $2a$ is the width of the contact region (x-direction) and $p_{\rm fluid}(t)$ the average fluid pressure in the nominal contact region. Combining the two equations above gives

$$\frac{{\rm d}\bar{u}}{{\rm d}t} = -\frac{\bar{u}^3\phi_{\rm p}(\bar{u})}{4\eta a^2}p_{\rm fluid}(t). \tag{14}$$

If p_0 is the applied pressure acting on the top surface of the block, we have

$$p_{\rm fluid}(t) = p_0 - p_{\rm cont}(t), \tag{15}$$

where $p_{\rm cont}$ is the (locally, or ensemble averaged) asperity contact pressure. If the pressure p_0 is so small that for all times $\bar{u} \gg h_{\rm rms}$, then in this case $\phi_{\rm p}(\bar{u}) \approx 1$. For $\bar{u} \gg h_{\rm rms}$ we also have [7]

$$p_{\rm cont} \approx \beta E^* \exp\left(-\frac{\bar{u}}{u_0}\right), \tag{16}$$

where $E^* = E/(1-\nu^2)$ (here E is the Young's modulus and ν the Poisson ratio), and $u_0 = h_{\rm rms}/\alpha$. The parameters α and β depend on the fractal properties of the rough surface [7].

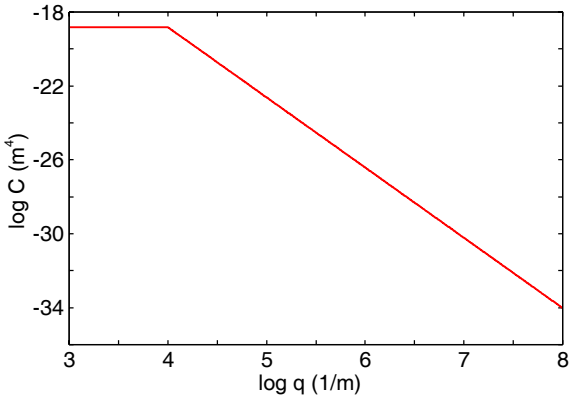

Fig. 4. (Color online) The logarithm (with 10 as basis) of angular average power spectrum as a function of the logarithm of the wave vector. For $q_{\rm r} < q < q_1$, with the roll-off wave vector $q_{\rm r} = 10^4{\rm m}^{-1}$ and the cut-off wave vector $q_1 = 10^8{\rm m}^{-1}$, the surface is self-affine fractal with the Hurst exponent $H = 0.9$. The low wave vector cut-off $q_0 = 10^3{\rm m}^{-1}$ and $h_{\rm rms} = 10$ μm.

At high enough squeezing pressures and after long enough time, the interfacial separation will be smaller than $h_{\rm rms}$, so that the asymptotic relation (16) will no longer hold. In this case the relation $p_{\rm cont}(\bar{u})$ can be calculated using the equations given in ref. [8]. Substituting (15) in (14) and measuring pressure in unit of p_0, separation in unit of $h_{\rm rms}$ and time in unit of the relaxation time

$$\tau = \frac{4\eta a^2 u_0}{h_{\rm rms}^3 p_0} = \frac{4\eta a^2}{\alpha h_{\rm rms}^2 p_0}, \tag{17}$$

one obtains

$$\frac{{\rm d}\bar{u}}{{\rm d}t} \approx -\alpha^{-1}\phi_{\rm p}(\bar{u})\bar{u}^3(1-p_{\rm cont}), \tag{18}$$

where $\alpha = h_{\rm rms}/u_0$. In order to study the squeeze-out over a large time period, $t_0 < t < t_1$, it is convenient to write $t = t_0 e^{\mu}$ ($0 < \mu < \mu_1$ with $\mu_1 = \ln(t_1/t_0)$). In this case (18) takes the form

$$\frac{{\rm d}\bar{u}}{{\rm d}\mu} \approx -\alpha^{-1}t\phi_{\rm p}(\bar{u})\bar{u}^3(1-p_{\rm cont}). \tag{19}$$

This equation, together with the relation $p_{\rm cont}(\bar{u})$, constitutes two equations for two unknowns ($\bar{u}$ and $p_{\rm cont}$) which can be easily solved by numerical integration.

We have studied the influence of percolation on the fluid squeeze-out for an elastic solid with randomly rough surface squeezed against a rigid flat surface in a fluid with the viscosity $\eta = 12$ Pa s. In most of the studies the rough surface has the power spectrum shown in fig. 4 with the root-mean-square roughness $h_{\rm rms} = 10$ μm and the large wave vector cut-off $q_1 = 10^8$ m^{-1}. We also present some results for another surface with $q_1 = 10^7$ m^{-1}. The elastic block has rectangular shape with the width $2a = 1.84$ cm (x-direction) and infinite length (y-direction), and the squeezing pressure $p_0 = 2$ MPa. The rubber has the Young's modulus $E = 3$ MPa and Poisson ratio $\nu = 0.5$.

DOCKET ALARM

Explore Litigation Insights

Docket Alarm provides insights to develop a more informed litigation strategy and the peace of mind of knowing you're on top of things.

Real-Time Litigation Alerts

Keep your litigation team up-to-date with **real-time alerts** and advanced team management tools built for the enterprise, all while greatly reducing PACER spend.

Our comprehensive service means we can handle Federal, State, and Administrative courts across the country.

Advanced Docket Research

With over 230 million records, Docket Alarm's cloud-native docket research platform finds what other services can't. Coverage includes Federal, State, plus PTAB, TTAB, ITC and NLRB decisions, all in one place.

Identify arguments that have been successful in the past with full text, pinpoint searching. Link to case law cited within any court document via Fastcase.

Analytics At Your Fingertips

Learn what happened the last time a particular judge, opposing counsel or company faced cases similar to yours.

Advanced out-of-the-box PTAB and TTAB analytics are always at your fingertips.

API

Docket Alarm offers a powerful API (application programming interface) to developers that want to integrate case filings into their apps.

LAW FIRMS
Build custom dashboards for your attorneys and clients with live data direct from the court.

Automate many repetitive legal tasks like conflict checks, document management, and marketing.

FINANCIAL INSTITUTIONS
Litigation and bankruptcy checks for companies and debtors.

E-DISCOVERY AND LEGAL VENDORS
Sync your system to PACER to automate legal marketing.